Reaction Kinetics, Mechanisms and Catalysis (2022) 135:1607–1620
https://doi.org/10.1007/s11144-022-02219-5

Facile and template-free synthesis of nano-macroporous $LaCoO_3$ perovskite oxide for efficient diesel soot oxidation

Neha[1] · **Satya Vir Singh**[1]

Received: 12 January 2022 / Accepted: 30 March 2022 / Published online: 5 April 2022

Abstract

The basic $LaCoO_3$ perovskite oxides were prepared by the series of methods (reverse co-precipitation, citric acid aided sol–gel, glycine assisted solution combustion), underwent physicochemical characterization (XRD, FTIR, BET, XPS and SEM), followed by their soot oxidation activity tests in both "loose" and "tight" conditions of soot-catalyst contact. The activity tests revealed that the $LaCoO_3$ catalyst formed using glycine assisted combustion synthesis gives the best performance with the T_{10}, T_{50}, and T_{90} at 361 °C, 404 °C and 445 °C, respectively, in loose contact conditions and T_{10}, T_{50}, and T_{90} at 306 °C, 330 °C and 355 °C, respectively, in tight contact conditions. Its outstanding performance can be attributed to its unique morphology consisting of scaffolds having an extensively interconnected macroporous network with macropores having nanoporous struts as walls as evidenced by SEM results. Such morphology makes the active sites of inner pores accessible to the gaseous (air) as well solid reactant (soot particles), thereby benefitting soot oxidation reaction.

Keywords Nano-macroporous · Glycine · Soot oxidation · $LaCoO_3$ · Scaffold

Introduction

The emission of particulate matter (mainly soot) from diesel-fueled engines causes harmful health and environmental impact, necessitating its control [1]. The noble metal-catalyzed diesel particulate filters (CDPF) are commercially used for soot removal, though the high cost of noble metals necessitates the need to explore alternative materials such as transition metal oxides (TMOs). Among TMOs, perovskite-type complex metal oxides ABO_3, where A usually stands for a rare earth metal with 12 coordinated cations and B stands for a transition metal, has been widely studied and

✉ Neha
neha.rs.che16@itbhu.ac.in

[1] Department of Chemical Engineering, Indian Institute of Technology (BHU), Varanasi 221005, India

employed in catalytic soot oxidation. The perovskite-type oxides have been reported to exhibit soot oxidation activity at par with noble metal-based catalysts under favorable conditions owing to their high reducibility, thermochemical stability, and high oxidizing ability of B site cation [2–5]. However, in general, their low specific surface area and pore size limit their soot oxidation performance. Over the years, advances in catalyst preparation techniques have led to the development of nanometric perovskites with very high specific surface areas [6, 7]. The nanometric perovskites possessing high specific surface area reported to be very efficient for soot combustion as their high surface area enhances contact points between catalyst and soot [7]. However, in such a catalyst, only the external surface of the catalyst gets involved in making contact with soot particles. The internal surface (inside surface of pores) of the catalyst is not able to make contact with the soot particles due to the low diameter of the pores (< 10 nm). The soot particles, which generally have a diameter > 25 nm [8] can't enter the low diameter of their pores (< 10 nm).

To overcome this issue, researchers over the years have shifted their focus to interconnected macroporous structures. In interconnected macroporous structures, the large pores (> 50 nm) [5, 9, 10] can permit the entering of soot particles inside its pores, making active sites of inner pores accessible to soot particles. Further, in recent studies, the presence of mesopores along with macropores in the catalytic structures exhibit synergistic effect, where ordered macroporous framework facilitated the diffusion and mass transfer of soot particles, mesoporous parts of the framework are beneficial for activation of gaseous reactants (NO, O_2) [11]. The reported methods for the synthesis of ordered macroporous structures involves the use of the template, which makes the preparation process complex and multistep in nature. In template free synthesis, the formation of disordered meso-macroporous structures by combination of ethylene glycol-ligation and solution combustion technique for use as soot oxidation catalyst is reported in recent literature [5].

Based on the literature, it can be concluded that the meso-macroporous structures are beneficial for soot oxidation, though the synthesis process is a challenge. As mesopores are mainly involved in boosting gas diffusion, the nanopores instead of mesopores can also be anticipated to do this work. Till date, nano-macroporous structures have not been investigated for soot oxidation application. Therefore, an attempt has been made to fabricate $LaCoO_3$ nano-macroporous structure via facile and cost-effective template free synthesis method, involving the use of glycine as combustion assistant as well as pore forming agent. For comparison, two other conventional methods, such as co-precipitation method (CP) [12] and citric acid assisted sol–gel synthesis (SG) [12, 13] were also used for $LaCoO_3$ preparation. The physiochemical characteristics of the synthesized catalysts were analyzed by XRD, FTIR, BET, SEM, and XPS and tested for soot oxidation.

Experimental

Catalyst preparation

Reverse co-precipitation method

Equimolar amounts of $La(NO_3)_3{\cdot}6H_2O$ and $Co(NO_3)_2{\cdot}6H_2O$ were dissolved in water forming 2.75 M solution at 65 °C and then immediately dropped into Na_2CO_3 solution (1.4 M, pH 9, 65 °C), leading to precipitation of cations. The Na_2CO_3 to nitrate solution in 2:1 volume ratio is taken to ensure desired pH. After filtering, the precipitates were dried overnight at 120 °C and then calcined in air at 750 °C (5 °C min^{-1}) for 4 h, denoted as $LaCoO_3$-CP in manuscript.

Citric acid aided sol–gel method

Equimolar amounts of $La(NO_3)_3{\cdot}6H_2O$ and $Co(NO_3)_2{\cdot}6H_2O$ (each 5 mmol) were mixed and dissolved in 50 ml of DI water. 10 mmol of citric acid monohydrate (CA), corresponding to a CA/Co + La nitrates molar ratio of 2, was added to the dissolved nitrates under continuous stirring for ~ 20 min at room temperature until a colloidal sol was formed. The obtained sol was heated in an oil bath at 80 °C under continuous stirring for ~ 5 h, resulting in transparent gel. In next step, the as-prepared gel was dried overnight in an oven at 120 °C and a loose and foamy pink colored organic solid precursor was obtained on drying. The organic precursor underwent two step calcination process, where the precursor was firstly calcined at 450 °C for 2 h (2 °C min^{-1}) to remove the organics and then, the temperature was increased to 750 °C for 4 h (5 °C min^{-1}) to obtain final catalyst denoted as $LaCoO_3$-SG in the manuscript.

Glycine assisted combustion synthesis

Stoichiometric amounts of $La(NO_3)_3{\cdot}6H_2O$ and $Co(NO_3)_2{\cdot}6H_2O$ were dissolved in 2% glycine aqueous solution (w/v) and intimately mixed via magnetic stirrer at room temperature for 24 h to form a stable gel. After that, the gel containing beaker was immediately placed on a preheated hot plate (300 °C), where mixture gets ignited and a fast and explosive reaction took place within few minutes, resulting in foamy shiny grey colored precursor, denoted as $LaCoO_3$-GCP in manuscript. The precursor was further calcined at 750 °C for 4 h to obtain to generate a pure phase metal oxide catalyst, denoted as $LaCoO_3$-GC.

Characterization

The structural analysis was carried out by performing X-Ray diffraction (XRD) on Rigaku Miniflex 600 with CuK_{α} ($\lambda = 1.5406$ Å) radiation, a scan rate of 6° min^{-1}, a voltage of 40 kV, and a current of 15 mA over the scan range of 20°–80°.

The perovskite structural formation examination was done by performing Fourier Transform Infrared Spectroscopy (FT-IR) in the 400–4500 cm^{-1} region on Nicolet iS5 spectrometer (Thermo Scientific™) instrument equipped with DTGS KBr detector.

The surface morphologies of the samples were determined using FEI Nova 600 field emission SEM operated at 15 kV accelerating voltage.

The N_2 adsorption–desorption isotherms of the catalysts were obtained at 77 K on Belsorp mini II analyzer (MicrotracBEL Corp.). Their specific surface areas were measured following the Brunauer–Emmett–Teller (BET) method, and their pore size distribution isotherms were derived from the N_2 adsorption isotherms based on Barrett Joyner Halenda (BJH) model.

X-ray photoelectron spectra (XPS) data was obtained on a X-ray photoelectron spectrometer (Thermo Fisher Scientific K-alpha system) with a with monochromated Kα source at 1400.0 eV. The C1s peak at 284.8 eV of contaminant carbon was taken as a reference to correct the binding energy scale. All samples were pretreated for 15 s with argon to exclude surface impurities. XPS data was collected and processed using the Thermo Avantage XPS software package. Features such as the area and position of multi-components in a XPS spectra were extracted using ORIGIN software. Curve fitting was typically achieved with a Gaussian component. Semi-quantitative analysis accounted for a linear background subtraction.

Evaluation of the catalytic performance

Instead of using commercially available Printex-U (Degussa), a commonly used model soot for conducting diesel soot oxidation related experiments, diesel soot was prepared in the Lab, details of its preparation are given under supplementary information S1. Its physicochemical characteristics (using XRD, FT-IR, SEM–EDX) were also studied and compared with that of Printex-U (Degussa) and real diesel soot (soot emitted from diesel engines under practical conditions) [14]. The physicochemical properties of the Lab prepared diesel soot as given under supporting information (S3) were found to be comparable with that of Printex-U (Degussa) and real diesel soot, suggesting the suitability of using Lab prepared diesel soot for conducting experiments (Fig. S1).

The samples to be used for activity testing are prepared as follows: (a) Loose contact samples: gentle mixing of 100 mg catalyst and 25 mg soot with a spatula for about 2 min; (b) Tight contact samples: rigorous mixing of 100 mg catalyst and 25 mg soot using agate mortar for ~ 15 min. Further, the soot oxidation catalytic activity of the prepared samples was tested by conducting temperature programmed oxidation (TPO) procedure on a fixed-bed tubular quartz microreactor ($\Phi = 6.0$ mm),

embedded with a K-type thermocouple to record the real-time temperature of the catalyst bed. Each TPO procedure ran from ambient temperature to temperature corresponding to complete soot oxidation (heating rate of 2 °C min^{-1}) in an air at a total flow rate of 100 ml min^{-1}. Further, the concentration measurements of the outlet gases (CO and CO_2) with an on-line gas chromatograph (GC, 5765 Nucon) equipped with a thermal conductivity detector (TCD) and a flame ionization detector (FID). A negligible amount of CO is detected, compared with CO_2, in all cases indicating the very high CO_2 selectivity. The catalytic activity was evaluated by the T_{10}, T_{50} and T_{90} values obtained during TPO runs, which were the temperatures corresponding to 10%, 50% and 90% conversion of soot.

Determination of activation energy

The activation energy (E_a) for soot oxidation in air over samples was calculated under tight contact following Ozawa method based on Eq. (1) [10]:

$$\ln\ \phi = C - 0.4567\left(\frac{E_a}{RT_\alpha}\right) \tag{1}$$

Here ϕ, E_a, R, T_α and C is the heating rate, the apparent activation energy, the gas constant, and the temperature at α (here it is 50%) of soot oxidized, constant depending on the reaction, respectively.

A weighed amount of prepared sample consisting of catalyst-soot tight-contact mixture in 4:1 ratio, was transferred to a TGA crucible under the influence of air at 40 ml min^{-1}, heated from ambient temperature to 700 °C with different heating rates (2, 5, and 10 °C). Then, the E_a was estimated from the slope of the plotted $1/T_\alpha$ – ln ϕ line.

Results and discussion

XRD and FTIR studies

The phase analysis from the obtained XRD patterns, as shown in Fig. 1, of the catalyst samples revealed the presence of the rhombohedral $LaCoO_3$ (*) phase (JCPDS 48-0123) as the major phase in all the samples [15]. In $LaCoO_3$-CP sample, besides major reflections characteristic of $LaCoO_3$ phase, few weak reflection corresponding to the hexagonal $La(OH)_3$ (o) phase (JCPDS 36-1481) [16], amounting to the less crystalline nature of the sample. The presence of $La(OH)_3$ peaks indicate that the given calcination temperature is not high enough to fully decompose the precipitates. However, a compromise is required as further high-temperature calcination can cause significant sintering of the sample and major loss of surface area as evidenced by SEM and BET results in later sections.

The XRD patterns, as given in Fig. S2 of the dark grey colored precursor formed from glycine combustion (before calcination) showed comparatively less crystallinity in comparison to its final catalyst $LaCoO_3$-GC (after calcination). Besides the

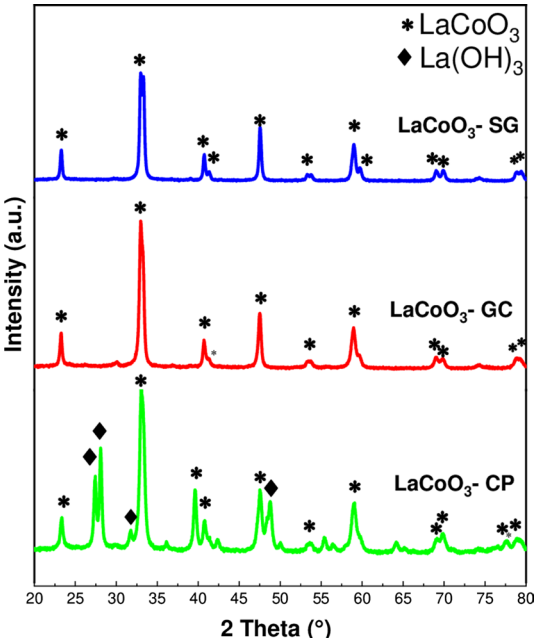

Fig. 1 X-ray diffraction patterns of the $LaCoO_3$-CP, $LaCoO_3$-GC and $LaCoO_3$-SG perovskites prepared via co-precipitation, glycine combustion and sol–gel, respectively followed by air calcination at 750 °C. Almost all peaks from all the patterns are ascribed to $LaCoO_3$ perovskite structure (JCPDS 48-0123) and very few to $La(OH)_3$ (JCPDS 36-1481) from $LaCoO_3$-CP

reason of lack of sufficient combustion temperature to form dominant crystalline structure, the incomplete combustion process could also be the reason behind less crystallinity. The grey color of the formed precursor supports the latter. The unavailability of sufficient oxygen during combustion results in the formation of carbon residue with zero value of enthalpy leading to the reduction of the total enthalpy of reaction and adiabatic temperature (less exothermicity) resulting in weakly crystalline structure instead of highly anticipated crystalline form owing to high combustion enthalpy fuel molecule in glycine [17]. The residual carbon atoms in the product phase (precursor) found to be useful for achieving the desired morphology, as will be discussed in detail in later Sect. 3.3. The further calcination of the precursor at higher temperature of 750 °C ($LaCoO_3$-GC catalyst) results in the formation of crystalline form $LaCoO_3$ as shown in Fig. 1, confirming that the given 750 °C temperature was sufficient to achieve full crystallization. Associated gas evolution during the calcination process provides highly porous framework. Further, $LaCoO_3$-SG sample also exhibited crystalline structure as revealed by its crystallite size (Table 1)

Table 1 Specific surface area, pore volume and crystallite size of the $LaCoO_3$ samples prepared by different methods

Catalyst	Specific surface area ($m^2\ g^{-1}$)	Pore volume ($cm^3\ g^{-1}$)	Crystallite size[a] (nm)
$LaCoO_3$-CP	11.13	0.040	12.96
$LaCoO_3$-SG	7.0	0.026	13.53
$LaCoO_3$-GC	3.92	0.029	14.93

[a]Measured using the Scherrer equation

most probably due to the sintering of the particles as the local temperature increases during the combustion of organics (citric acid here) in calcination process. The sintering results in the loss of surface area, as evidenced by subsequent BET and SEM analysis given under Sects. 3.2 and 3.3.

In addition to XRD analysis, FT-IR analysis also confirms the formation of $LaCoO_3$ perovskite structure in all samples. As shown in Fig. S3, all the samples showed the intense peak at ~ 600 cm^{-1} which is a characteristic peak for the MO_6 octahedra generally found in perovskite (ABO_3) oxide [18]. Another weak peak at 420 cm^{-1} signifies the formation of O–Co–O and La–O-Co, indicating that $LaCoO_3$ structure was generated. Expectedly, besides above mentioned peaks, a sharp peak at 3610 cm^{-1} is attributed O–H asymmetry stretching vibration in the hydroxides [19] is also observed in the case of $LaCoO_3$-CP catalyst, confirming the presence of $La(OH)_3$ phase in the catalyst.

BET studies

Figs. 2A, B and S4 show the N_2 adsorption–desorption isotherms and the pore-size distributions curves of the as-synthesized catalysts, respectively, and their corresponding BET surface areas and pore volumes are summarized in Table 1. As can be observed from Fig. 2A, $LaCoO_3$-GC sample displayed a typical type-I N_2 sorption isotherms, providing indication of presence of macropores in the catalyst [20]. Its pore size distribution curve (Fig. 2B) based on BJH method showed the presence of nanopores within the so called mesopore range (2–25 nm, according to the IUPAC classification). Furthermore, the wide diameter range (0–200 nm) of d*V*/d(log*D*) pore volumes, indicate the abundance of both nanopores (0–10 nm) and macropores (50–200 nm) in $LaCoO_3$-GC catalyst. In addition, the observance of variation tendency of dV/d(logD) in the pore size range of 1–10 nm of $LaCoO_3$-GC catalyst also indicates the presence of a nanopores in the catalyst. In the catalytic oxidation of soot, as the particles size is usually > 25 nm, the catalyst with pore sizes > 25 nm can easily facilitate the soot–catalyst contact, critical for the catalytic soot oxidation

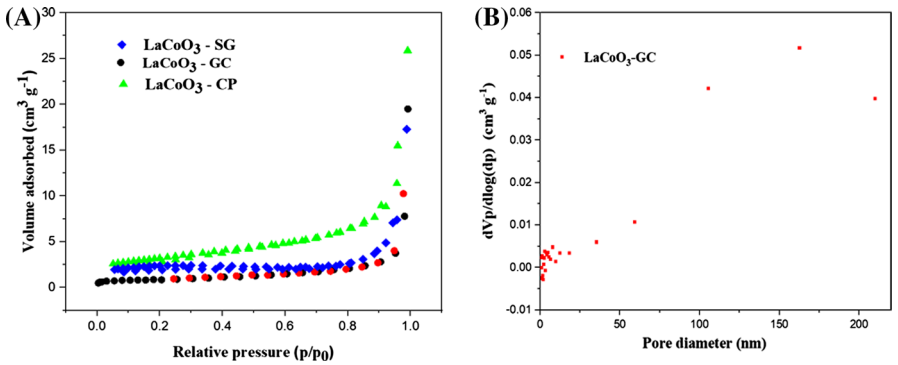

Fig. 2 BET N_2-adsorption isotherms of the $LaCoO_3$-CP, $LaCoO_3$-GC and $LaCoO_3$-SG perovskites; measurements were performed at standard temperature and pressure (STP) (273.15 K and atmospheric pressure (1.013×10^5 Pa) (**A**) and pore size distribution of $LaCoO_3$-CP (**B**)

reaction to occur effectively. At the same time, the radius of the reactants (NO and O_2) used in the reaction is small, hence, can utilize pore having sizes < 25 nm for their diffusion to reach active sites as well as to come in contact with soot particles. Though, the > 25 nm pores could also be utilized by gas reactants to reach active sites, but there are fair chances of the > 25 nm pores getting partially blocked by soot particles. Hence, the hybrid pore structure as exhibited by $LaCoO_3$-GC catalyst is highly beneficial for enhancing its catalytic soot oxidation performance.

In terms of specific surface areas, as expected owing to its weakly crystalline nature, $LaCoO_3$-CP sample exhibited the highest surface area of 11.13 $m^2\ g^{-1}$, owing to its small particle size, as evidenced by SEM results later. The $LaCoO_3$-SG sample also exhibited a high surface area of 7.01 $m^2\ g^{-1}$ owing to its porous structure as can be seen in SEM images below. $LaCoO_3$-GC exhibited the lowest surface area of 3.92 $m^2\ g^{-1}$, most probably due to the sintering caused due to the dramatic release of energy during spontaneous combustion of the solution during its preparation process. The instant release of energy causes severe sintering of the particles, letting sintered particles to take the form of scaffolds, as shown in SEM images below.

SEM results

The surface morphology of all the catalyst samples was studied through SEM. The micrograph of $LaCoO_3$-CP as given in Fig. S5A reveals that the uniform, almost spherical nanoparticles having a narrow size distribution range, with weak particle agglomeration, are dominant. Besides this, highly agglomerated small lumps can be seen at certain regions, most probably due to the presence of undecomposed $La(OH)_3$ precipitates in the sample, correlating with the XRD and FTIR outcomes. The SEM micrograph of the $LaCoO_3$-SG sample, as shown in Fig. S5B, revealed evenly distributed nanoscaled fine spherical particles which are clustered together owing to agglomeration, resulting in incorporated sheet-like fragments embedded in the particle matrix [15].

Interestingly, the $LaCoO_3$-GC sample showed quite distinct morphology, where scaffolds separated by interconnected macropores (> 50 nm) was observed. Fig. S5 shows the (C) low- and (D) high-magnification micrographs of precursor (denoted as

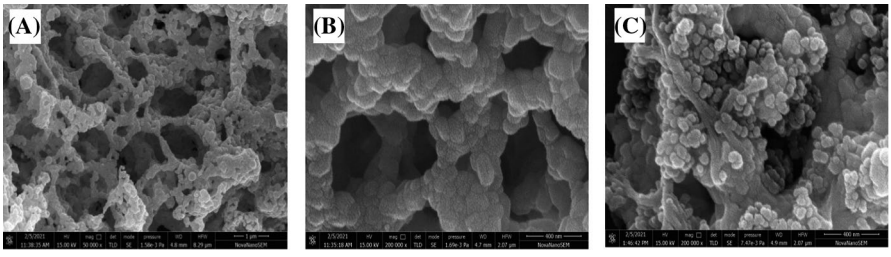

Fig. 3 SEM images of $LaCoO_3$-GC obtained after air calcination of the precursor formed by instantaneous combustion of nitrate salts with glycine (**A** and **B**), and loose contact mixture of $LaCoO_3$-GC catalyst with lab prepared diesel soot (**C**)

$LaCoO_3$-GCP) formed at 300 °C through the solution combustion synthesis, where highly sintered (non-porous) scaffolds separated by macropores was observed. The change in the morphology of the non-porous scaffolds can be observed in Fig. 3A low- and 3B high-magnification SEM images of final catalyst ($LaCoO_3$-GC) obtained after calcination of the precursor at 750 °C for 2 h. After calcination, the surface of the scaffolds became rough, and pores were formed, though the scaffolds remain intact and did not collapse, resulting in interconnected macroporous structure. The porous scaffolds were generated most probably during the removal of remaining glycine in the precursor. The presence of high number of carbon atoms in glycine fuel and very short period of instantaneous combustion causes unavailability of oxygen for carbon atoms in glycine fuel, resulting in incomplete combustion or combustion with residual carbon atoms in the formed precursor. These residual carbon atoms further get removed during calcination performed in air at slow heating rate. The FT-IR analysis of $LaCoO_3$-GCP (Fig. S2) showed a peak at 1385 confirm the presence of $C_2H_4NO_2^{-1}$ (glycinate ion). Further, the grey color of the as-obtained glycine combusted sample was also reported probably due to the remaining glycine in the sample [21]. The above-explained role played by glycine in changing morphology verified that the here, the glycine also act as the pore-forming agent in addition to its main role as combustion agent (fuel) [13]. The large pore sizes (> 50 nm) and interconnected framework achieved in this case certainly have the potential of achieving better diffusion of solid soot particles in the inner pores and high adsorb-activation capacity for gas reactants [11]. As shown in Fig. S2, the lab prepared diesel soot particles with particle size > 25 nm, demands big inner pores for their better diffusion. When loosely mixed the $LaCoO_3$-GC catalyst and soot in 5:1 weight ratio is observed as shown as in Fig. 3C, it can be seen that many soot particles (small and bright spherical particles) stucked together forming soot clusters are easily got diffused into the inner space of the catalyst. The easy diffusion of soot clusters into the macropores, resulting in effective utilization of both external and internal surface of the catalysts, thereby improving chances of the contact between reactants and active sites [5, 10].

Based on the morphological characteristics shown by $LaCoO_3$-GC in contact with soot, it can be concluded that the macroporous framework is desirable for the effective diffusion of solid soot particles and gaseous flow. The easy access of reactants to the active sites can definitely improve the solid–solid contact efficiency. Further, the nanoporous surface formed on the walls of scaffolds nanostructure makes inner active sites accessible to the molecular gas reactants. The active sites adsorb these gas reactants and transform them efficiently to the effective intermediate species, which facilitate the diffusion of molecular reactants as well as boost the indirect contact efficiency during reaction process. Having advantages of both macroporous and nanoporous surfaces in single framework, the nano-macroporous $LaCoO_3$-GC could be a highly potential catalyst for soot combustion reaction.

XPS analysis

In order to investigate the effect of chemical composition and oxidation states of various $LaCoO_3$ perovskite samples on their oxidation performance, XPS analysis

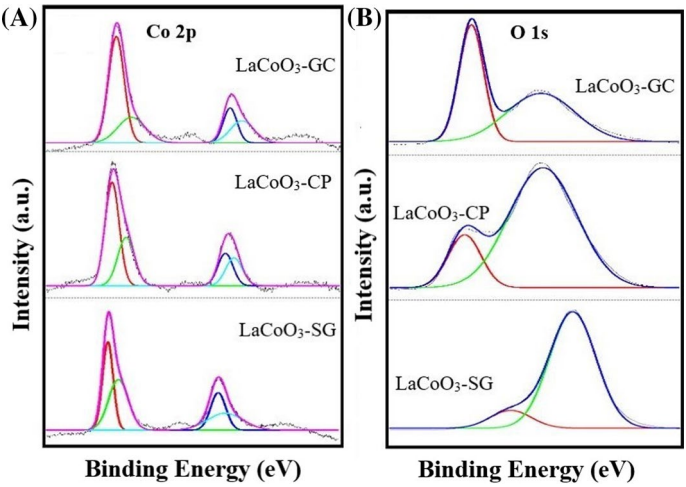

Fig. 4 The detailed high-resolution Co 2p (**A**) and O 1s spectra (**B**) of $LaCoO_3$-CP, $LaCoO_3$-SG, and $LaCoO_3$-GC perovskites. Curve fitting was done using Origin Software

Table 2 Values of Co^{3+}, Co^{2+}, O_L, and O_A, for $LaCoO_3$-CP, $LaCoO_3$-SG, and $LaCoO_3$-GC perovskites (area%)

Catalyst	Co^{3+}	Co^{2+}	O_L	O_A
$LaCoO_3$-SG	68.52	36.48	27.22	72.78
$LaCoO_3$-CP	75.64	24.36	17.35	55.65
$LaCoO_3$-GC	60.45	39.55	46.44	59.56

was done. Fig. S6 shows the overall XPS survey spectrum of all the samples and as expected, it clearly revealed the existence of La, Co, O, C elements in all the samples. Further, the XPS spectra with related individual high-resolution element analysis were further analyzed to obtain the information of chemical states. In the deconvoluted high-resolution Co 2p spectra, as given in Fig. 4A, the peaks at ~ 779 eV and at ~ 794 eV could be attributed to Co $2p_{3/2}$ and Co $2p_{1/2}$ of Co^{3+}. The fitted peaks at ~ 781 eV and at ~ 795 eV could be assigned to Co $2p_{3/2}$ and Co $2p_{1/2}$ of Co^{2+}. The incomplete diffusion of Co ions during processing of Co ions into La_2O_3 to form $LaCoO_3$ perovskite could be the reason behind the observance of Co^{2+} ions in the samples. From the Co^{3+} and Co^{2+} content values summarized in Table 2, where the Co^{3+} content values reflect the oxidation ability of the catalyst, the Co^{3+} content increases in the order as follows $LaCoO_3$-GC < $LaCoO_3$-SG < $LaCoO_3$-CP.

As given in Fig. 4B, the O 1s spectra is fitted with two peaks at ~ 528 eV and ~ 531 eV, corresponding to lattice oxygen (O_L) and surface adsorbed oxygen (O_A), respectively [22, 23]. Noticeably, the O_A is related to oxygen vacancy, consisted of electrophilic oxygen species such as O_2^-, O_2^{2-} or O^-, exhibits a higher mobility, than their respective O_L [24]. Thus, the relative content of adsorbed oxygen vacancies (O_A) and lattice oxygen (O_L) of the catalysts as given under Table 1 is taken as a parameter to evaluate their catalytic activities. Their respective O_A content was found in the order as follows: $LaCoO_3$-CP > $LaCoO_3$-SG > $LaCoO_3$-GC.

The observance of significant variation in O_A content for the different catalysts could be due to the enhancement of Co^{3+}. As previous studies have reported that the surface adsorbed oxygen vacancy (O_A) can accelerate the ions translation on their (sub-) surface with lower energy barrier [25], the Co atom transferred the internal charges to the surface adsorbed oxygen species causing enrichment of Co^{3+} and O_A. The highest O_A content in $LaCoO_3$-CP indicated its good oxygen adsorption capability and additionally $LaCoO_3$-CP also provides the highest specific surface area which can also significantly enhance the adsorption capability of oxygen. Therefore, $LaCoO_3$-CP perovskite exhibited appreciable CO and soot oxidation activity owing to its high surface area and high mobility of the oxygen adsorbed vacancies. However, as explained in introduction, the soot oxidation reaction is highly dependent on the proximity of contact between soot and catalyst particles, which was invariably achieved by morphology formed in $LaCoO_3$-GC catalyst, as explained in SEM analysis in detail, the morphology effect was found to be more dominant when it comes to soot oxidation activity of the prepared catalysts. Therefore, the $LaCoO_3$-GC catalyst exhibited better soot oxidation than the $LaCoO_3$-CP and $LaCoO_3$-GC catalyst as further discussed in later section below.

Further, the examination of the C 1s spectra, as given in Fig. S7, revealed the peak at 289.4 eV suggest the presence of carbonates species in all the samples (Table S1). The more extensive formation of these species is observed in case of $LaCoO_3$-CP, suggesting the association of concentration of these chemisorbed carbon-containing species (Table S1) with the specific surface area (Table 1). The high prevalence of carbonate species generally corresponds to high specific surface area and probably higher oxygen mobility, as also evidenced by the results of previously reported literature [26].

The La 3d XPS spectra (Fig. S8) are also presented for convenience. Though, as La has stable oxidation state and does not participate in the reaction as active site, no special efforts have been made in detailed explanation.

Soot oxidation activity

The activity results of the prepared $LaCoO_3$ catalysts towards soot oxidation in air under both tight and loose contact conditions are shown in Fig. 5, and the corresponding T_{10}, T_{50}, T_{90} and CO_2 values are summarized in Table S2. Same soot activity order is followed in case of both loose as well as tight contact conditions and the order is as follows: $LaCoO_3$-GC (T_{90} = (TC) & (LC)) > $LaCoO_3$-CP (T_{90} = (TC) & (LC)) > $LaCoO_3$-SG (T_{90} = (TC) & (LC)). Our most promising $LaCoO_3$-GC catalyst achieved complete soot oxidation (T_{100}) at 369 °C and 480 °C in tight and loose contact mode, respectively.

To study the intrinsic catalytic activities of the $LaCoO_3$ catalyst samples, a series of TGA experiments were performed to calculate their apparent activation energy for soot oxidation. As expected, (Fig. S9), the activation energy (Ea) also follows the same order as follows: $LaCoO_3$-GC (64 kJ mol^{-1}) > $LaCoO_3$-CP (80 kJ mol^{-1}) > $LaCoO_3$-SG (83 kJ mol^{-1}). The catalytic activity evaluation results showed that $LaCoO_3$-GC catalyst samples exhibited the highest performance

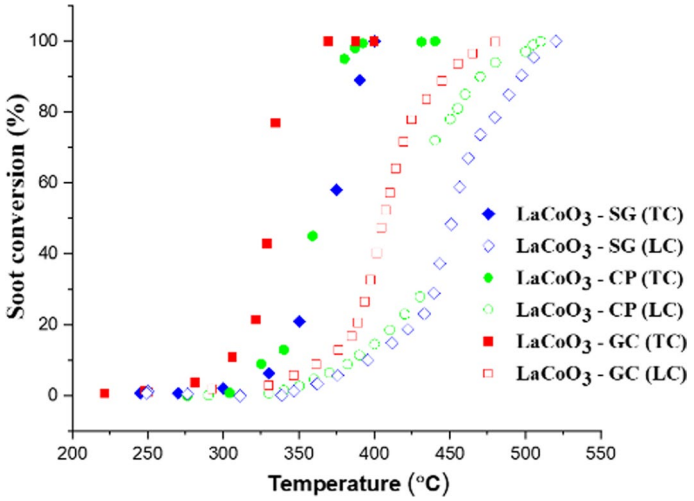

Fig. 5 Catalytic soot conversion curves recorded for the $LaCoO_3$-GC, $LaCoO_3$-CP and $LaCoO_3$-SG perovskites in both "loose" and "tight" contact conditions with soot (soot:catalyst ratio = 1:4, in the flow of synthetic air 100 ml min^{-1})

with the lowest activation energy (Ea = 64 kJ mol^{-1}) for soot oxidation, indicating its better intrinsic activity.

Conclusions

$LaCoO_3$ perovskite prepared by co-precipitation, sol–gel, and glycine-assisted solution combustion techniques were tested for the soot oxidation activity in the air under both "loose" and "tight" contact conditions. The as-prepared catalysts by different methods mainly showed variation in their morphological characteristics and catalytic soot oxidation activity. The $LaCoO_3$ catalyst prepared by glycine-assisted solution combustion method showed a distinct interconnected macroporous structure, the highest catalytic soot oxidation catalytic activity, and the lowest activation energy of 64 kJ mol^{-1} in tight contact mode. The macroporous structure of the catalyst found to be highly desirable for the soot combustion reaction, as the macropores with > 50 nm average diameter let the soot particles enter the inner pores, unleashing the inner surface area of the catalysts available for reaction to take place, thereby, benefitting soot oxidation reaction.

Supplementary Information The online version contains supplementary material available at https://doi.org/10.1007/s11144-022-02219-5.

Acknowledgements The authors dedicate this work to the late Prof. Dr. Ram Prasad (IIT (BHU)), who succumbed to covid-19, everyone knew him as an excellent teacher and outstanding human being. The authors acknowledge the CIF IIT (BHU), India, for providing a characterization facility to carry out the research work.

References

1. Adamska K, Smykała S, Zieliński S et al (2021) Oxidation of soot over supported RuRe nanoparticles prepared by the microwave-polyol method. Reac Kinet Mech Cat 134:221–242. https://doi.org/10.1007/s11144-021-02048-y
2. Wu X, Ran R, Weng D (2009) NO_2-aided soot oxidation on $LaMn_{0.7}Ni_{0.3}O_3$ Perovkite-type catalyst. Catal Lett 131:494–499. https://doi.org/10.1007/s10562-009-9917-y
3. Uppara HP, Dasari H, Singh SK et al (2019) Effect of copper doping over $GdFeO_3$ Perovskite on soot oxidation activity. Catal Lett 149:3097–3110. https://doi.org/10.1007/s10562-019-02843-2
4. Zhao M, Liu J, Liu J et al (2020) Fabrication of $La_{1-x}Ca_xFeO_3$ perovskite-type oxides with macro-mesoporous structure via a dual-template method for highly efficient soot combustion. J Rare Earths 38:369–375. https://doi.org/10.1016/j.jre.2019.06.009
5. Zhang G, Zhao Z, Liu J et al (2009) Macroporous perovskite-type complex oxide catalysts of $La_{1-x}K_xCo_{1-y}Fe_yO_3$ for diesel soot combustion. J Rare Earths 27:955–960. https://doi.org/10.1016/S1002-0721(08)60369-5
6. Wang H, Zhao Z, Liang P et al (2008) Highly active $La_{1-x}K_xCoO_3$ perovskite-type complex oxide catalysts for the simultaneous removal of diesel soot and nitrogen oxides under loose contact conditions. Catal Lett 124:91–99. https://doi.org/10.1007/s10562-008-9429-1
7. Wang H, Zhao Z, Xu C, Liu J (2005) Nanometric $La_{1-x}K_xMnO_3$ perovskite-type oxides—highly active catalysts for the combustion of diesel soot particle under loose contact conditions. Catal Lett 102:251–256. https://doi.org/10.1007/s10562-005-5864-4
8. Stanmore BR, Brilhac J-F, Gilot P (2001) The oxidation of soot: a review of experiments, mechanisms and models. Carbon 39:2247–2268. https://doi.org/10.1016/S0008-6223(01)00109-9
9. Feng N, Chen C, Meng J et al (2016) Facile synthesis of three-dimensionally ordered macroporous silicon-doped $La_{0.8}K_{0.2}CoO_3$ perovskite catalysts for soot combustion. Catal Sci Technol 6:7718–7728. https://doi.org/10.1039/C6CY00677A
10. Feng Z, Liu Q, Chen Y et al (2017) Macroporous $SmMn_2O_5$ mullite for NOx-assisted soot combustion. Catal Sci Technol 7:838–847. https://doi.org/10.1039/C6CY02478E
11. Xiong J, Zhang P, Li Y et al (2021) Ordered macro-mesoporous nanostructure of Pd/ZrO2 catalyst for boosting catalytic NO-assisted soot oxidation. Chem Eng Sci 239:116635. https://doi.org/10.1016/j.ces.2021.116635
12. Mishra A, Prasad R (2015) Effect of preparation method and calcination temperature on $LaCoO_3$ perovskite catalyst for diesel soot oxidation. Can Chem Trans 3:95–107. https://doi.org/10.13179/canchemtrans.2015.03.01.0168
13. Kim J, Chen X, Shih PC, Yang H (2017) Porous perovskite-type lanthanum cobaltite as electrocatalysts toward oxygen evolution reaction. ACS Sustain Chem Eng 5:10910–10917. https://doi.org/10.1021/acssuschemeng.7b02815
14. Neeft JPA, van Pruissen OP, Makkee M, Moulijn JA (1995) Catalytic oxidation of diesel soot: Catalyst development. In: Frennet A, Bastin J-MBT-S in SS and C (eds) Catalysis and automotive pollution control III. Elsevier, pp 549–561
15. Natile MM, Ugel E, Maccato C, Glisenti A (2007) $LaCoO_3$: effect of synthesis conditions on properties and reactivity. Appl Catal B 72:351–362. https://doi.org/10.1016/j.apcatb.2006.11.011
16. Hu BC, Liu H, Dong W et al (2007) $La(OH)_3$ and La_2O_3 nanobelts -synthesis and physical properties. Adv Mater 19:470–474. https://doi.org/10.1002/adma.200601300
17. Sadabadi H, Allahkaram SR, Kordijazi A et al (2021) Structural characterization of $LaCoO_3$ perovskite nanoparticles synthesized by sol-gel autocombustion method. Eng Rep 3:e12335. https://doi.org/10.1002/eng2.12335
18. Sun M, Jiang Y, Li F et al (2010) Dye degradation activity and stability of perovskite-type $LaCoO_{3-x}$ (x=0~0.075). Mater Trans 51:2208–2214. https://doi.org/10.2320/matertrans.M2010200
19. Zhu H, Yang D, Yang H et al (2008) Reductive hydrothermal synthesis of La(OH)3:Tb3+ nanorods as a new green emitting phosphor. J Nanoparticle Res 10:307–312. https://doi.org/10.1007/s11051-007-9250-6
20. Yang W, Dong Y, Li J et al (2021) Templating synthesis of hierarchically meso/macroporous N-doped microalgae derived biocarbon as oxygen reduction reaction catalyst for microbial fuel cells. Int J Hydrogen Energy 46:2530–2542. https://doi.org/10.1016/j.ijhydene.2020.10.087
21. Sherikar B, Umarji A (2013) Synthesis of diopside by solution combustion process using glycine fuel. Int J Mod Phys Conf Ser 22:217–223. https://doi.org/10.1142/S2010194513010155

22. Ao R, Ma L, Guo Z et al (2021) Effects of the preparation method on the simultaneous catalytic oxidation performances of $LaCoO_3$ perovskites for NO and Hg^0. Fuel 305:121617. https://doi.org/10.1016/j.fuel.2021.121617
23. Dacquin JP, Lancelot C, Dujardin C et al (2009) Influence of preparation methods of $LaCoO_3$ on the catalytic performances in the decomposition of N_2O. Appl Catal B 91:596–604. https://doi.org/10.1016/j.apcatb.2009.06.032
24. Ansari AA, Adil SF, Alam M et al (2020) Catalytic performance of the Ce-doped $LaCoO_3$ perovskite nanoparticles. Sci Rep 10:15012. https://doi.org/10.1038/s41598-020-71869-z
25. Chen S, Jiang H, Cheng Q et al (2021) Amorphous vanadium oxides with metallic character for asymmetric supercapacitors. Chem Eng J 403:126380. https://doi.org/10.1016/j.cej.2020.126380
26. Kang M, Park ED, Kim JM, Yie JE (2007) Manganese oxide catalysts for NOx reduction with NH_3 at low temperatures. Appl Catal A 327:261–269. https://doi.org/10.1016/j.apcata.2007.05.024